International Journal of Heat and Mass Transfer 55 (2012) 5275–5288

Contents lists available at SciVerse ScienceDirect

International Journal of Heat and Mass Transfer

journal homepage: www.elsevier.com/locate/ijhmt

A two-energy equation model for dynamic heat and mass transfer in an adsorbent bed using silica gel/water pair

İsmail Solmuş [a,*,1], D. Andrew S. Rees [b], Cemil Yamalı [a], Derek Baker [a]

[a] Department of Mechanical Engineering, Middle East Technical University, 06531 Ankara, Turkey
[b] Department of Mechanical Engineering, University of Bath, Claverton Down, Bath BA2 7AY, UK

ARTICLE INFO

Article history:
Received 20 December 2011
Received in revised form 11 May 2012
Accepted 15 May 2012
Available online 2 June 2012

Keywords:
Adsorption
Cooling
Silica/gel
LDF
LTNE

ABSTRACT

In this study, the influence of the adsorbent bed dimensions, convective heat transfer coefficient between the cooling fluid and adsorbent bed and the thermal conductivity of the solid adsorbent material on the transient distributions of the solid and gas phase temperature difference, differences in the adsorbate concentration predicted by the instantaneous equilibrium and linear driving force (LDF) models, solid phase temperature, gas pressure and adsorbate concentration inside the adsorbent bed of a solid sorption cooling system have been investigated numerically for a nearly isobaric adsorption process. Silica gel/water is selected as the working pair. A transient two-dimensional local thermal non-equilibrium model has been developed that takes into account both internal and external mass transfer resistances. The local volume averaging method has been used to derive the macro-scale governing conservation equations from the micro-scale equations. It has been found that generally, the effects of the parameters investigated on the transient distributions of the temperature difference between the phases, difference in adsorbate concentration between the instantaneous equilibrium and LDF models, and gas phase pressure gradients are negligible small. The thickness of the adsorbent bed for the given adsorbent bed length and thermal conductivity of the solid adsorbent material have a large influence on the transient distributions of the solid phase temperature and adsorbate concentration. On the other hand, the transient temperature and adsorbate concentration distributions are only slightly affected by the variation of the adsorbent bed length and convective heat transfer for the conditions studied.

1. Introduction

Traditional air-conditioning technologies can have numerous adverse impacts due to both the energy they consume and the refrigerants used including the following: contributing to environmental problems such as climate change, ozone depletion, and pollution [1–6]; contributing to infrastructure problems by stressing the electric generating, transmission and distribution infrastructure by increasing the peak demand for electricity [2]; contributing to economic problems through the cost of supplying this energy [2,3]; contributing to reducing energy security problems if energy must be imported to meet this demand [5]. Thermally driven cooling systems powered using solar energy or waste heat such as absorption, adsorption, and desiccant systems have the potential to reduce or eliminate many of these problems [4,6]. The present work is focused on adsorption cooling systems. Dieng and Wang provide an excellent overview of this technology [7]. The heart of this technology is a thermal compression process using an adsorbent bed that replaces the mechanical compression process in a vapor-compression cycle. This adsorbent bed is alternately cooled and heated, which in turn alternately causes the bed to adsorb refrigerant at a low pressure and desorb refrigerant at high pressure, thus producing a thermally powered compression process.

The overall performance of thermal powered adsorption cooling (TPAC) systems is typically limited by heat and mass transfer limitations inside the adsorbent bed due to the poor thermal conductivity of the solid adsorbent, and internal (intraparticle) and external (interparticle) mass transfer resistances. Therefore, many attempts have been made to improve the heat and mass transfer characteristics of the adsorbent beds for a TPAC system. However, reducing heat transfer resistances inside a bed tends to increase the mass transfer resistances and vice versa. Therefore, heat and mass transfer conditions inside the adsorbent bed need to be understood well to design a high performance adsorbent bed. Over the past few decades, various mathematical models have been developed to understand the heat or heat and mass transfer mechanism inside the adsorbent bed of TPAC systems. These models are summarized in Table 1 in terms of their important characteristics and their most important characteristics in terms of the present

* Corresponding author. Tel.: +90 3122105276; fax: +90 3122102536.
E-mail addresses: er24dem@hotmail.com, solmus@metu.edu.tr (İ. Solmuş).
[1] On leave of absence from Department of Mechanical Engineering, Atatürk University, 25240 Erzurum, Turkey.

0017-9310/$ - see front matter © 2012 Elsevier Ltd. All rights reserved.
http://dx.doi.org/10.1016/j.ijheatmasstransfer.2012.05.036

Nomenclature

a_v	area of gas–solid interface per unit volume, m^{-1}
C_p	specific heat, J kg^{-1} K^{-1}
D_e	equivalent diffusivity in the adsorbent particles, m^2 s^{-1}
D_o	reference diffusivity, m^2 s^{-1}
d_p	average diameter of the adsorbent particle, m
E_a	activation energy of surface diffusion, J mol^{-1}
h	convective heat transfer coefficient between the adsorbent bed and cooling fluid, W m^{-2} K^{-1}
h_{gs}	interfacial convective heat transfer coefficient, W m^{-2} K^{-1}
K	permeability, m^2
k_m	mass transfer coefficient within the adsorbent particles, s^{-1}
k	thermal conductivity, W m^{-1} K^{-1}
L	length of the adsorbent bed, m
Nu_d	Nusselt number
P	pressure, kPa
Pr	Prandtl number
Q	heat of adsorption, J kg_w^{-1}
R	universal gas constant, J mol^{-1} K^{-1}
Re_d	Reynolds number
R_g	specific gas constant for water vapor, J kg^{-1} K^{-1}
R_i	inner diameter of the adsorbent bed, m
R_o	outer diameter of the adsorbent bed, m
r	radial coordinate, m
T	temperature, K
t	time, s
v_r	gas phase velocity in radial direction, m s^{-1}
v_z	gas phase velocity in axial direction, m s^{-1}
X	adsorbate concentration, kg_w kg_{ad}^{-1}
X_∞	equilibrium adsorption capacity, kg_w kg_{ad}^{-1}
z	axial coordinate, m

Greek symbols

μ	viscosity, Ns m^{-2}
ρ	density, kg m^{-3}
ε_t	total porosity
ε_b	bed porosity
ε_p	particle porosity
λ_{g_e}	effective thermal conductivity for the gas phase, W m^{-1} K^{-1}
λ_{s_e}	effective thermal conductivity for the solid phase, W m^{-1} K^{-1}

Subscripts

c	cooling
co	condenser
e	evaporator
g	gas phase
re	regeneration
i	initial
s	solid phase
sat	saturation

research are as follows. The equations were proposed for the heat transfer within a porous medium typically assuming a mobile gas (vapor) phase, an immobile solid phase (adsorbed adsorbate + adsorbent), and Local Thermal Equilibrium (LTE) between the gas and solid phases. However, LTE assumption is no longer valid in some circumstances [8] and thus, an energy equation for each phase needs to be developed, i.e., Local Thermal Non-Equilibrium (LTNE). The adsorbate gas flow from a solid adsorbent particle surface to inner points of the particle and through the voids between the solid adsorbent particles are generally referred to as internal and external mass transfer, respectively. The resistance to internal mass transfer is typically predicted using the Linear Driving Force (LDF) or Solid Diffusion (SD) models. Occasionally, resistance to this type of flow is neglected and adsorption equilibrium is assumed. This assumption is reasonably good for adsorbent particles with small diameters. Darcy's or Ergun's equation is used widely to account for the resistance to external mass transfer. On the other hand, in these models external mass transfer resistances are often ignored and a uniform pressure is assumed, especially if the permeability of the bed or/and working pressure of the adsorbate is high.

Table 1
Classification of the existing mathematical models in terms of their important characteristics.

References	Dimension	Internal mass transfer resistance model	External mass transfer resistance model	Energy equation
[9–11]	3D	LDF	Darcy's equation	LTE
[12,13]	1D	LDF	Uniform pressure	LTE
[12,13]	1D	SD	Uniform pressure	LTE
[12–14]	1D	Adsorption equilibrium	Uniform pressure	LTE
[15–19]	2D	LDF	Darcy's equation	LTE
[20,21]	2D	Adsorption equilibrium	Ergun's equation	LTE
[23]	2D	LDF	Uniform pressure	LTE
[24]	0D (Lumped)	LDF	Uniform pressure	LTE
[25,26]	2D	LDF	Darcy's equation	LTE and LTNE
[22,27]	2D	Adsorption equilibrium	Uniform pressure	LTE
[28]	1D	Adsorption equilibrium	Darcy's equation	LTE
[29]	1D	LDF	Darcy's equation	LTE

These previous studies show that even though the performance of TPAC units have been widely studied for different design parameters and operating conditions [9–24], little attention has been focused on investigating the transient heat and mass transfer behavior of the adsorbent bed of the TPAC units [25–29].

Mhimid [25] studied the heat and mass transfer in a zeolite bed during water desorption using the LTE and LTNE models and the results showed that the LTE assumption is not valid in regions with high rates of heat transfer (at the wall where external heating occurs, in the region where the vaporization takes place). Jemni and Nasrallah [26] investigated transient heat and mass transfer in a metal-hydrogen reactor and they concluded that the LTE model is not valid in the whole reactor. Guilleminot and Meunier [27] investigated numerically and experimentally heat and mass transfer in a non-isothermal fixed bed solid adsorbent reactor and they concluded that the uniform pressure model is more realistic than the uniform temperature models proposed previously. Yong and Sumathy [28] compared heat transfer only and combined heat and mass transfer models for transport processes in an adsorbent bed and they proposed two general criteria to perform an order of magnitude analysis to determine when the simpler heat transfer only model is appropriate. Demir et al. [29] performed a numerical study to investigate the effects of porosity on heat and mass transfer in a granular adsorbent bed and they found that the distributions of temperature and adsorbate concentration are strongly influenced by the bed porosity.

The objective of the present work is to perform a numerical study to investigate the dynamic behavior of the adsorbent bed of an adsorption cooling unit during the adsorption process. A transient two-dimensional LTNE model that accounts for both internal and external mass transfer resistances has been developed using the local volume averaging method. Most of the models proposed previously assume LTE between the vapor and solid phases without fully justifying the validity of this assumption. Therefore, one of the innovative points of this study is to compare the predictions resulting from the LTNE and LTE models to better understand when LTE can be assumed.

2. Description of the adsorbent bed

A schematic view of the adsorbent bed using the silica-gel/water working pair is shown in Fig. 1. All the dimensions of the adsorbent bed and the thermo-physical properties of the silica-gel/water pair are presented in Table 2. The primary components of the adsorbent bed are an inner vacuum tube, a mass transfer tube, a larger tubular shell and a single top cover for the vacuum tube and the tubular shell. Silica-gel granules are packed in the annulus between the vacuum and mass transfer tubes and a vapor gap is left at the top of the vacuum tube to allow better vapor transfer in the axial direction. The vacuum tube is inserted into the larger tubular shell and a heat transfer fluid circulated between the shell and vacuum tube to cool down the adsorbent bed during the adsorption process. Refrigerant vapor enters the vacuum tube through the top cover and flows both in the radial and axial directions. The right hand side from the center line of the adsorbent bed represents the plots in the results.

3. Mathematical modeling

The 2D domain modeled is labeled as Modeling Domain in Fig. 1. The right and bottom edges are in thermal contact with the heat transfer fluid and are referred to as the heat transfer boundaries. The top and left edges are assumed to be well-insulated and are modeled as being adiabatic.

The adsorbent bed consisting of vapor adsorbate, adsorbed adsorbate, and solid adsorbent is a discontinuous medium and thus, it is not suitable for theoretical modeling. For this reason, the local volume averaging method has been used to model this discontinuous medium as a nearly continuous one. The details of this method can be found in references [8,30–32]. The governing macroscopic conservation equations are derived by taking the average of the microscopic ones over the averaging volume.

In this study, the combination of the adsorbed adsorbate and solid adsorbent are modeled as a single solid and are referred to collectively as the solid phase. The adsorbed adsorbate is considered as being immobile and in thermal equilibrium with the solid adsorbent, and its volume fraction is assumed negligible. The resulting model is therefore two-phase (vapor and solid) with single phase flow (vapor).

The mathematical model proposed in this study is primarily based on the following assumptions and simplifications:

- the size of the adsorbent particles and the bed porosity are spatially uniform;
- the adsorbate's vapor phase is assumed to be an ideal gas;
- radiative heat transfer, viscous dissipation and the work done by pressure changes are neglected;
- the surface porosity is considered to be equal to the total porosity;
- physical properties such as thermal conductivities, specific heat capacities and viscosity are not a function of temperature;
- the thickness of the outer walls for the vacuum tube are assumed to be very thin and hence, its thermal resistance is neglected.

3.1. Mass conservation equation

The macro-scale mass conservation equation for the adsorbate gas is written as:

$$\varepsilon_t \frac{\partial(\rho_g)}{\partial t} + \frac{1}{r}\frac{\partial(r\rho_g v_r)}{\partial r} + \frac{\partial(\rho_g v_z)}{\partial z} + (1-\varepsilon_t)\rho_s \frac{\partial X}{\partial t} = 0 \quad (1)$$

The dispersive transport term was neglected since it is generally very small compared with the convective term and this is based on the order of magnitude analysis given by [30]. The local volume-averaged velocity is assumed to be equal to the superficial or Darcy's velocity. The density of the vapor adsorbate was considered to be uniform within the averaging volume [8] and hence, the intrinsic phase average density was replaced with the point density while the equation above was derived from its micro scale form.

The volume fraction of the gas phase, ε_g, is assumed to be equal to the total porosity, ε_t, and is evaluated using [9],

$$\varepsilon_t = \varepsilon_b + (1-\varepsilon_b)\varepsilon_p \quad (2)$$

Finite internal mass transfer rates are modeled using the LDF model [9]. The adsorption rate is assumed equal to this internal mass transfer and therefore adsorption equilibrium is not assumed.

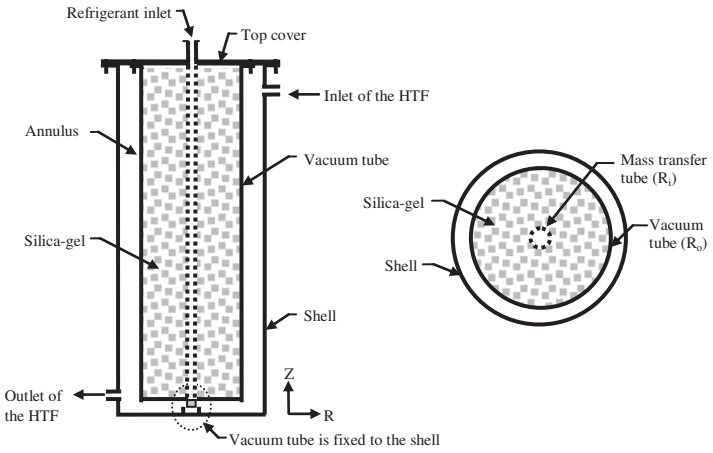

Fig. 1. A schematic view of the cylindrical adsorbent bed.

$$\frac{\partial X}{\partial t} = k_m(X_\infty - X) \tag{3}$$

Here k_m is the internal mass transfer coefficient given by:

$$k_m = 60\ D_e/d_p^2 \tag{4}$$

and D_e is the equivalent diffusivity in the adsorbent particles which is expressed as:

$$D_e = D_o \exp(-E_a/RT_s) \tag{5}$$

The equilibrium adsorption capacity of the adsorbent to the adsorbent's temperature and the adsorbate's pressure, i.e., $X = f(P, T_s)$, may be evaluated using the following modified Dubinin–Astakhov (D–A) equation [33].

$$X_\infty = 0.346 \exp[-5.6(T_s/T_{sat} - 1)^{1.6}] \tag{6}$$

3.2. Momentum equation

External mass transfer resistances are included in the present model, which can lead to significant bulk pressure gradients. Darcy's equation including only viscous effects is used to describe the velocity field of the vapor adsorbate in the computational domain. The inertial effects accounted for by Ergun's equation are ignored because of the very low speed of the vapor adsorbate flowing through the voids between the adsorbent particles.

$$v = -\frac{K}{\mu_g}\nabla P \tag{7}$$

Here K is the permeability which can be calculated by the following semi-emprical Blake-Kozeny equation,

$$K = \frac{d_p^2 \varepsilon_b^3}{150(1-\varepsilon_b)^2} \tag{8}$$

3.3. Energy conservation equations

During the energy transport inside the adsorbent bed, it was considered that local non thermal equilibrium between the gas and solid phases is significant. Therefore, two different energy conservation equations are developed to determine the separate temperature fields of the gas and solid phases.

3.3.1. Energy conservation equation for the gas phase

The macro scale energy conservation equation for the gas phase is written as:

$$C_{pg}\rho_g\left[\varepsilon_g\frac{\partial T_g}{\partial t} + v_r\frac{\partial T_g}{\partial r} + v_z\frac{\partial T_g}{\partial z}\right] + (1-\varepsilon_t)\rho_s\frac{\partial X}{\partial t}C_{pg}(T_s - T_g) = \frac{1}{r}\frac{\partial}{\partial r}\left(r\lambda_{g\_e}\frac{\partial T_g}{\partial r}\right) + \frac{\partial}{\partial z}\left(\lambda_{g\_e}\frac{\partial T_g}{\partial z}\right) + a_v h_{gs}(T_s - T_g) \tag{9}$$

The area-averaged temperatures are represented by volume-averaged temperatures. The intrinsic phase averages of density and temperature are represented by the point density and temperature, since the variation in the density and temperature over the averaging volume is considered to be very small [31].

3.3.2. Energy conservation equation for the solid phase

The local volume-averaged macroscopic energy conservation equation for the solid phase is derived in the same way as for the gas phase. It is given by:

$$\rho_s(1-\varepsilon_t)[C_{ps} + XC_{pw}]\frac{\partial T_s}{\partial t} = \frac{1}{r}\frac{\partial}{\partial r}\left(r\lambda_{s\_e}\frac{\partial T_s}{\partial r}\right) + \frac{\partial}{\partial z}\left(\lambda_{s\_e}\frac{\partial T_s}{\partial z}\right) - a_v h_{gs}(T_s - T_g) + (1-\varepsilon_t)\rho_s\frac{\partial X}{\partial t}Q \tag{10}$$

The fluid–solid specific surface area for spherical particles is determined by [25]:

$$a_v = 6(1-\varepsilon_t)/d_p \tag{11}$$

The interfacial heat transfer coefficient for the spherical particle is evaluated by [25]:

$$Nu_d = 2 + 1.8Pr^{0.33}Re_d^{0.5} \tag{12}$$

where, $Re_d = \rho_g v d_p/\mu_g$, $Nu_d = h_{gs}d_p/k_g$, $Pr = \mu_g C_{pg}/k_g$.

The equation of state for the adsorbate vapor phase is written as:

$$P = \rho_g R_g T_g \tag{13}$$

3.4. Initial and boundary conditions

Temperature, pressure and adsorbate concentration gradients are investigated where $T = T(t,r,z)$, $P = P(t,r,z)$, and $X = X(t,r,z)$.

The temperatures (solid and gas), pressure and adsorbate concentration distributions in both directions inside the adsorbent bed are initially considered to be uniform.

$$T_g(0,r,z) = T_s(0,r,z) = T_i, \quad P(0,r,z) = P_i, \quad X(0,r,z) = X_i \tag{14}$$

Referring to the analysis domain in Fig. 1, at the $r = R_i$ (left) and $z = L$ (top) boundaries it is assumed that the vapor pressure is equal to the evaporator pressure and the temperature gradients for both the solid and gas phases are zero (i.e., adiabatic boundaries).

$$P(t,R_i,z) = P_e \tag{15}$$

$$P(t,r,L) = P_e \tag{16}$$

$$\frac{\partial T_g}{\partial r}(t,R_i,z) = \frac{\partial T_s}{\partial r}(t,R_i,z) = 0 \tag{17}$$

$$\frac{\partial T_g}{\partial z}(t,r,L) = \frac{\partial T_s}{\partial z}(t,r,L) = 0 \tag{18}$$

At the $r = R_o$ (right) and $z = 0$ (bottom) boundaries the pressure gradient is zero since the walls are impermeable and a convective heat transfer boundary conditions exists for the solid and gas phases.

$$\frac{\partial P}{\partial r}(t,R_o,z) = 0 \tag{19}$$

$$\frac{\partial P}{\partial z}(t,r,0) = 0 \tag{20}$$

$$-\lambda_{g\_e}\frac{\partial T_g}{\partial r}(t,R_o,z) = h(T_g - T_c) \tag{21}$$

$$-\lambda_{s\_e}\frac{\partial T_s}{\partial r}(t,R_o,z) = h(T_s - T_c) \tag{22}$$

$$-\lambda_{g\_e}\frac{\partial T_g}{\partial z}(t,r,0) = h(T_g - T_c) \tag{23}$$

$$-\lambda_{s\_e}\frac{\partial T_s}{\partial z}(t,r,0) = h(T_s - T_c) \tag{24}$$

4. Solution procedure

The nonlinear coupled governing partial differential equations under consideration were solved numerically using the finite difference technique. The central differencing, first order upwind scheme, and forward differencing were used to discretize the second order spatial derivatives, convective, and unsteady terms, respectively. The resulting set of nonlinear algebraic equations was solved iteratively by the combination of the alternating direction implicit (ADI) method, the Newton–Raphson iteration scheme and a block tridiagonal matrix solver algorithm (Thomas algorithm). The grid distribution in the computational domain is uniform and nine algebraic equations were solved at each grid point. A computer simulation program based on the numerical procedure above was written in Matlab to perform the parametric investigation. In the simulation program, at each time step, iterations were terminated when the calculated difference between the two successive iterations of any dependent variable was $<10^{-6}$. The main simulation parameters used in the computer simulation program are given in Table 2.

The influence of the number of grid points and time steps on the solid phase temperature at nearly thermal equilibrium case and various locations in the computational domain is shown in Table 3. It can be seen from Table 3 that the difference between the results obtained for two different grid sizes ($5*25$ and $10*50$) and time steps (0.5 and 1 s) is quite small. Therefore, the number of grid points is varied in the range between $20*80$ and $25*100$ and the time step is selected as 0.25 s to ensure the reliability of the numerical computations.

Table 2
Main simulation parameters.

Parameter	Value	Unit	References
C_{pg}	1800	J kg^{-1} K^{-1}	
C_{ps}	924	J kg^{-1} K^{-1}	[34]
d_p	5e^{-4}	m	[34]
D_o	2.54e^{-4}	m^2 s^{-1}	[34]
E_a	4.2e^4	J mol^{-1}	[34]
h	100	W m^{-2} K^{-1}	
k_g	0.024	W m^{-1} K^{-1}	
k_s	0.198	W m^{-1} K^{-1}	[34]
L	0.1	m	
P_{co}	4.246	kPa	
P_e	1.228	kPa	
R_i	0.01	m	
R_o	0.02	m	
T_c	40	°C	
T_{re}	100	°C	
ε_b	0.37		[34]
ε_p	0.42		[34]
Q	2693	kJ kg^{-1}	[34]
μ_g	1.5e^{-5}	kg m^{-1} s^{-1}	[20]
ρ_s	2027	kg m^{-3}	[34]

Table 3
Effects of the number of grid points and time steps on the solid phase temperature (K) at nearly thermal equilibrium case and various locations in the computational domain.

		Δt = 0.5 s		Δt = 1 s	
		$5*25$	$10*50$	$5*25$	$10*50$
r, z (m)	0.012, 0.088	314,329935	314,379638	314,334036	314,383828
	0.018, 0.088	313,802534	313,845411	313,804846	313,847829
	0.012, 0.012	313,998231	314,032621	314,001147	314,035600
	0.018, 0.012	313,623038	313,652964	313,624663	313,654667

5. Results and discussion

The effect of the adsorbent bed dimensions in the axial and radial directions, the convective heat transfer coefficient and the thermal conductivity of the adsorbent material on the transient distributions of the temperature difference between the phases, the solid phase temperature, the pressure, the adsorbate concentration and the difference in the adsorbate concentration calculated from the instantaneous equilibrium and LDF models have been investigated numerically, and the results are presented below. For each parametric study all the parameters given in Table 2 are kept constant except the parameter investigated i.e., adsorbent bed length.

A schematic view of the isobaric adsorption process on a Clapeyron diagram is shown in Fig. 2. At the starting point of the adsorption process for all simulations (A), the adsorbate concentration, the solid and gas phase temperatures, and the pressure throughout the adsorbent bed are uniform and are equal to 0.2 $kg_w\ kg_{ad}^{-1}$, 348.5 K and 1.2282 kPa, respectively. At this point, the temperatures for the gas and solid phases were calculated by means of the regeneration temperature of the adsorbent bed (T_{re}), condenser pressure (P_{co}), and evaporator pressure (P_e) given in Table 2. The adsorption capacity of the solid adsorbent was assumed to be constant as the pressure inside the adsorbent bed was decreased from the condenser (P_{co}) to the evaporator (P_e) pressure. The adsorption process was terminated at point B where the adsorbent bed nearly reached thermal, mechanical and chemical equilibrium conditions and the values of the solid phase temperature, pressure and the adsorbate concentration throughout the adsorbent bed at this point (B) are presented in the Figs. 5–7 (3rd column) for various adsorbent bed lengths, respectively.

5.1. Temperature difference between the phases for the LTNE model

The temperature difference between the solid and gas phase inside the adsorbent bed was not taken into account in most of the studies published previously (see Table 1). Typically, in these studies, a single energy equation was used by assuming LTE between the phases without showing the validity of this assumption. However, it is stated in the literature [8] that this assumption may not be correct in some circumstances and it may lead to unrealistic simulation results. Therefore, one of the main objectives of this study is to investigate the validity of this assumption for the parameters investigated. For this purpose, two different energy

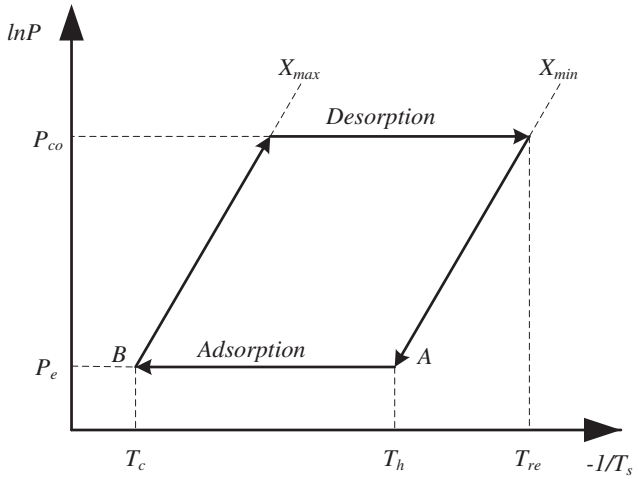

Fig. 2. A schematic view of the adsorption process on a Clapeyron diagram.

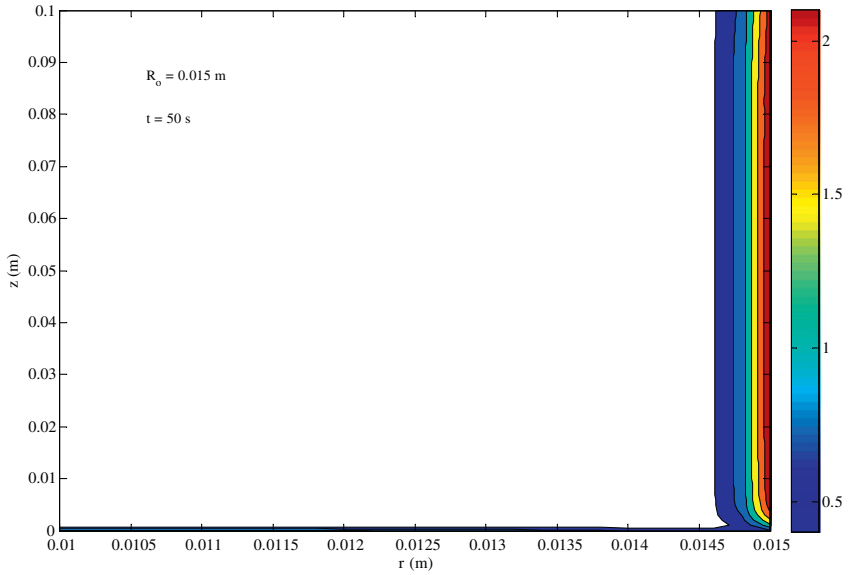

Fig. 3. The distribution of the temperature difference, K, between the solid and gas phases for the $R_o = 0.015$ m at $t = 50$ s.

conservation equations were developed to determine the separate temperature fields of the gas and solid adsorbent phases.

A parametric study of the transient distributions of the temperature difference between the solid and gas phases was performed for the following parameters and ranges: adsorbent bed length (0.05–0.2 m) and thickness (0.005–0.015 m); HTF convective heat transfer coefficient (25–400 W $m^{-2}K^{-1}$); and, thermal conductivity of the solid adsorbent material (0.2–1.5 W $m^{-1}K^{-1}$). For brevity only the condition of $R_o = 0.015$ m at $t = 50$ s is presented in Fig. 3 as this is representative of the other conditions. The heat transfer fluid flows past the right hand and bottom sides of Fig. 3, which results in large rates of heat transfer and temperature gradients at these boundaries. Conversely, the left and top sides are modeled as adiabatic boundary conditions and therefore the temperature gradients go to zero at these boundaries. Generally, the temperature difference between the phases is only significant (>4 °C) close to the outer boundaries exposed to the HTF, especially, during the first few seconds. However, this temperature difference typically becomes <4 °C for process times >50 s and decays toward zero as the time progress. The temperature difference between the phases at a given time increases with decreasing values of the adsorbent bed thickness and convective heat transfer coefficient and increasing values of the thermal conductivity of the solid adsorbent material, but is relatively insensitive to changes in adsorbent bed length. Therefore, it can be concluded that decreasing conductive and increasing convective thermal resistances resulting in low Biot number increases the temperature difference between the solid and gas phases. Consequently, the results obtained in this part of the study indicate that LTE assumption is reasonable for the range of conditions explored and thus, this assumption can be used for the simplicity.

5.2. Adsorbate concentration difference between the instantaneous equilibrium and LDF models

The difference in the adsorbate concentration distributions for the instantaneous equilibrium and LDF models for the various values of the adsorbent bed length and thickness, convective heat transfer coefficient and thermal conductivity of the solid adsorbent material are investigated and the range of values explored is the same for Section 5.1. The results presented in Fig. 4 are representative of the results for the other conditions and for brevity these other results are discussed but not presented graphically. The difference in adsorbate concentration between the instantaneous equilibrium and LDF models for all the parameters studied is generally negligible small and thus, typically, the instantaneous equilibrium adsorption model can be used instead of the LDF models for the modeling of the adsorbate concentration without leading to any significant computational errors under the given conditions. The difference in adsorbate concentration between the instantaneous equilibrium and LDF models decreases with increasing process time. This can be explained by the fact that the rate of adsorbate concentration calculated from the instantaneous equilibrium adsorption model is quite high at the early time steps of the process due to the high heat transfer rate and negligible pressure gradients and it decreases as time goes. On the other hand, the rate of adsorbate concentration computed from the LDF model is relatively slow at all times because of the internal mass transfer resistances. Therefore, initially, the adsorbate concentration difference between the instantaneous equilibrium and LDF models is relatively large and this difference decreases as time increases.

5.3. Adsorbent bed length

Isotherms of the solid phase, isobars and contours of the adsorbate concentration for adsorbent bed lengths of 0.05, 0.1 and 0.2 m and at times of 300, 900 and 1800 s are shown in Figs. 5–7, respectively. It is clear that the temperature, pressure and adsorbate concentration distributions inside the adsorbent bed is only slightly affected by variations in the adsorbent bed length for the given adsorbent bed thickness, especially for adsorbent bed lengths >0.1 m. The temperature and adsorbate concentration gradients in the axial direction are only significant near the bottom boundary at the early stages of the process. However, in the radial direction these gradients are not only considerable near the right heat transfer boundary but also throughout the rest of the bed. Temperature and adsorbate concentration gradients in both directions gradually become insignificant as the time progress. It can be concluded that the heat and mass transfer inside the adsorbent bed can be approximated as one dimensional in the r direction for large values of adsorbent bed length, but the two-dimensional effects cannot be neglected for aspect ratios nearly equal to one. The pressure gradients throughout the adsorbent bed are generally negligible. The

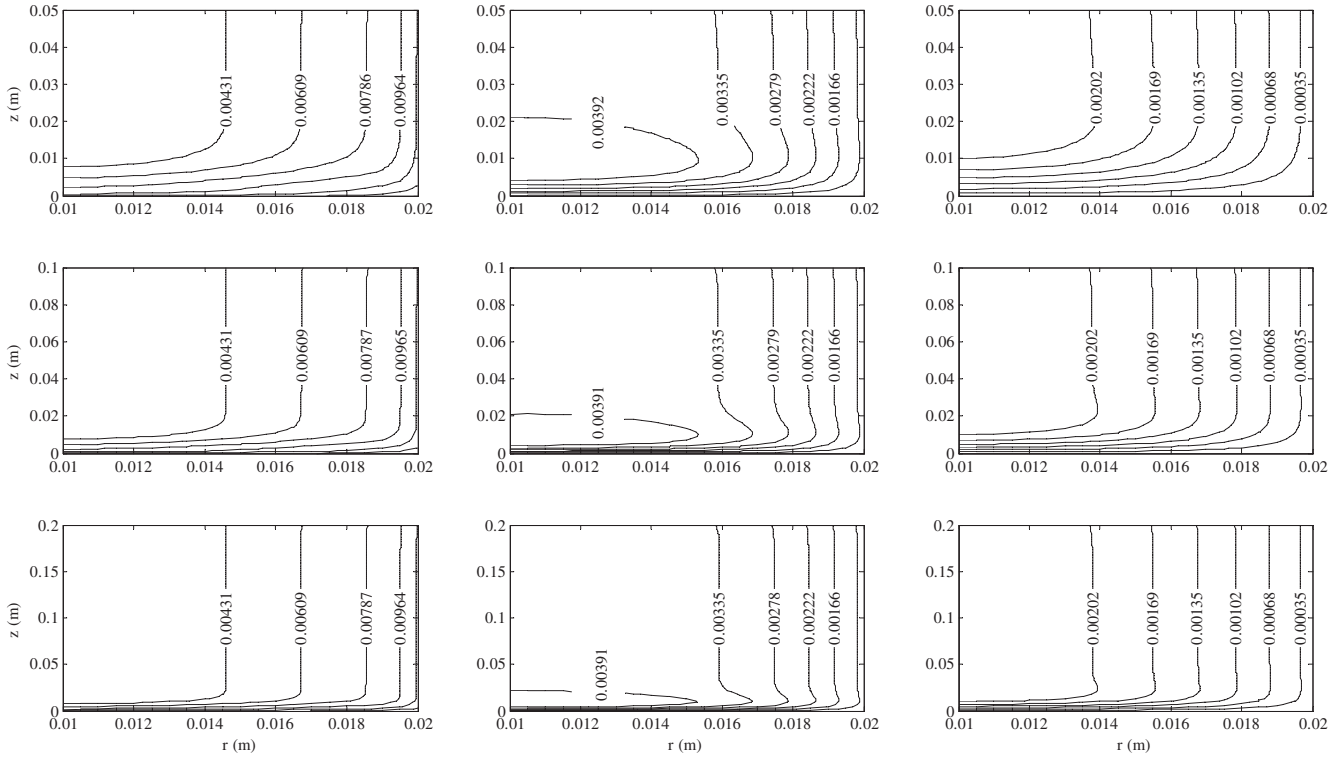

Fig. 4. The distribution of the adsorbate concentration difference between the equilibrium and LDF models, $kg_w\,kg_{ad}^{-1}$. [1st row $L = 0.05$ m, 2nd row $L = 0.1$ m, 3rd row $L = 0.2$ m and 1st column $t = 300$ s, 2nd column $t = 900$ s, 3rd column $t = 1800$ s.]

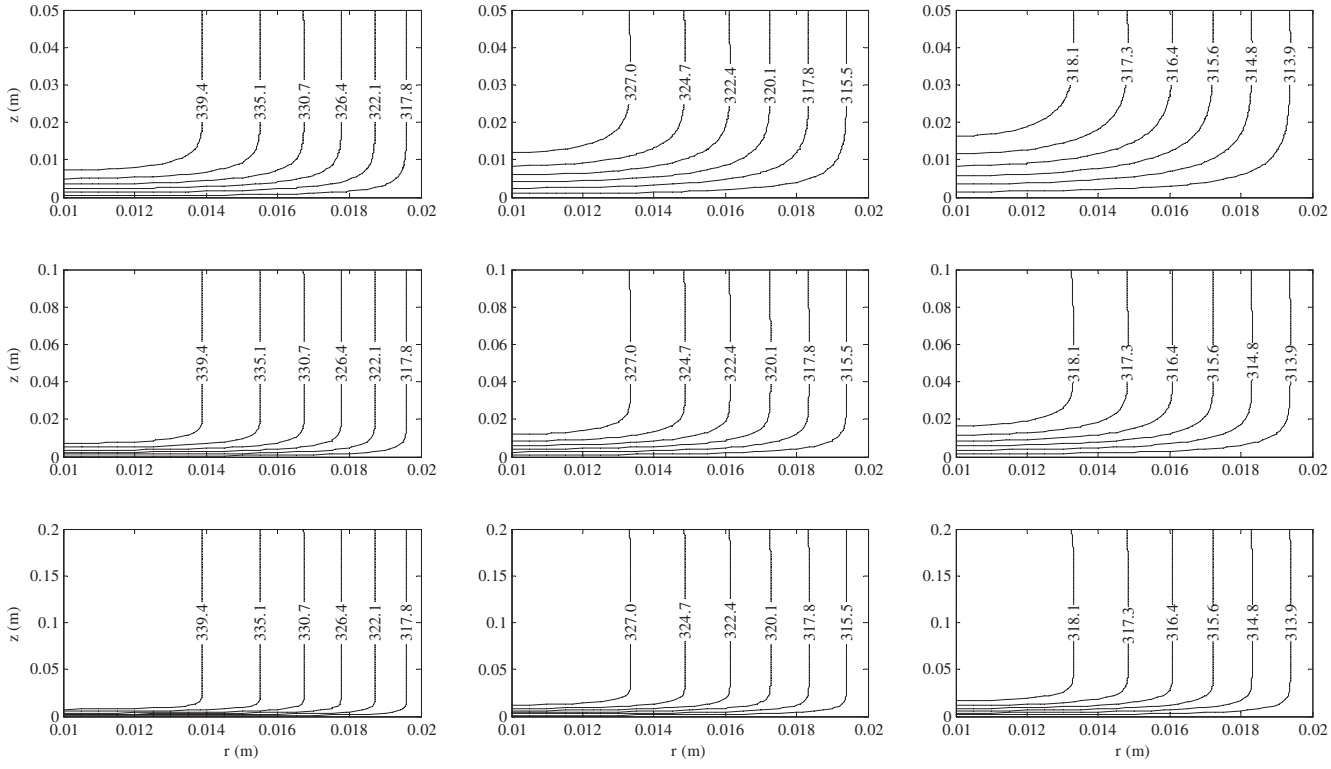

Fig. 5. Transient solid phase temperature, K, distribution for various adsorbent bed lengths. [1st row $L = 0.05$ m, 2nd row $L = 0.1$ m, 3rd row $L = 0.2$ m and 1st column $t = 300$ s, 2nd column $t = 900$ s, 3rd column $t = 1800$ s.]

resistance to adsorbate vapor flow in the axial direction is higher than that in the radial direction as a result of the high aspect ratio. Initially, the pressure at the heat transfer boundaries decreases suddenly due to increasing value of the adsorbate concentration since there is a sharp temperature drop at these boundaries. Thus, the adsorbate vapor in the interior of the adsorbent bed starts to

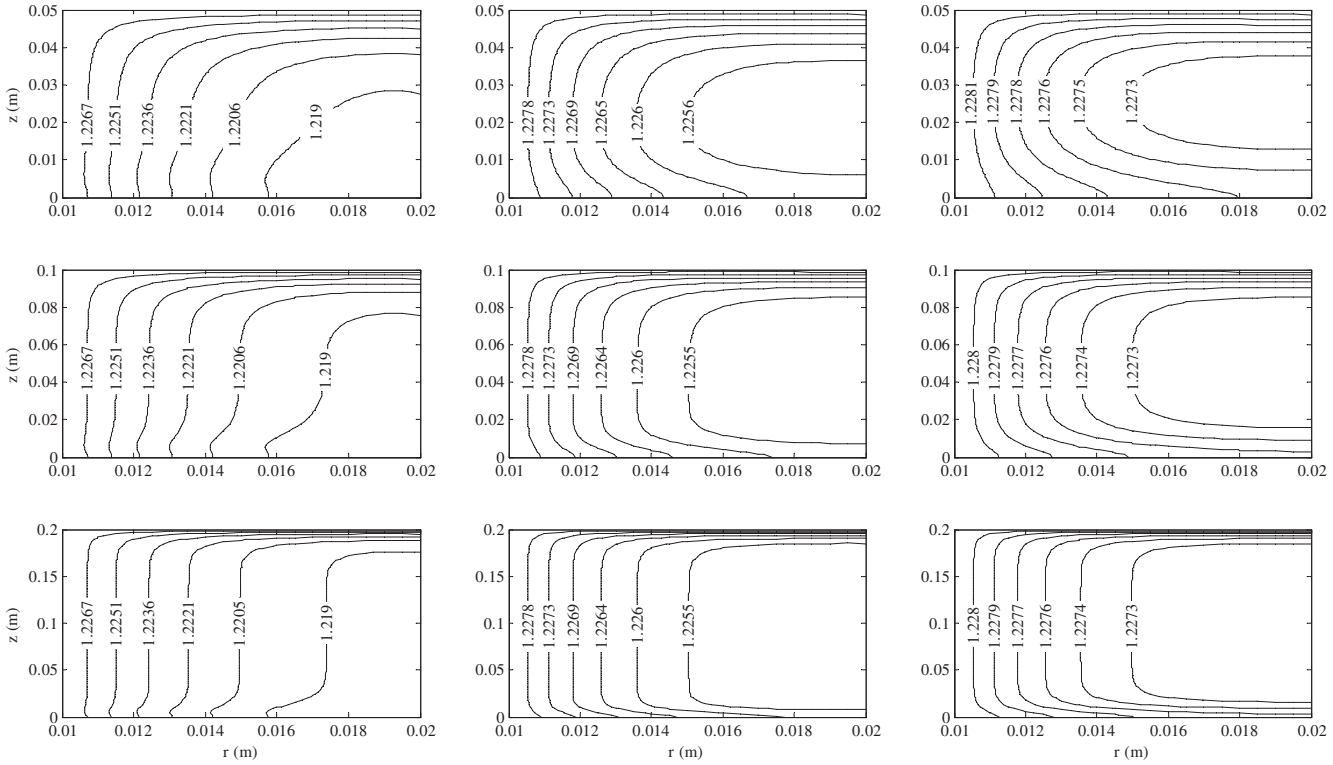

Fig. 6. Transient pressure, kPa, distribution for various adsorbent bed lengths. [1st row L = 0.05 m, 2nd row L = 0.1 m, 3rd row L = 0.2 m and 1st column t = 300 s, 2nd column t = 900 s, 3rd column t = 1800 s.]

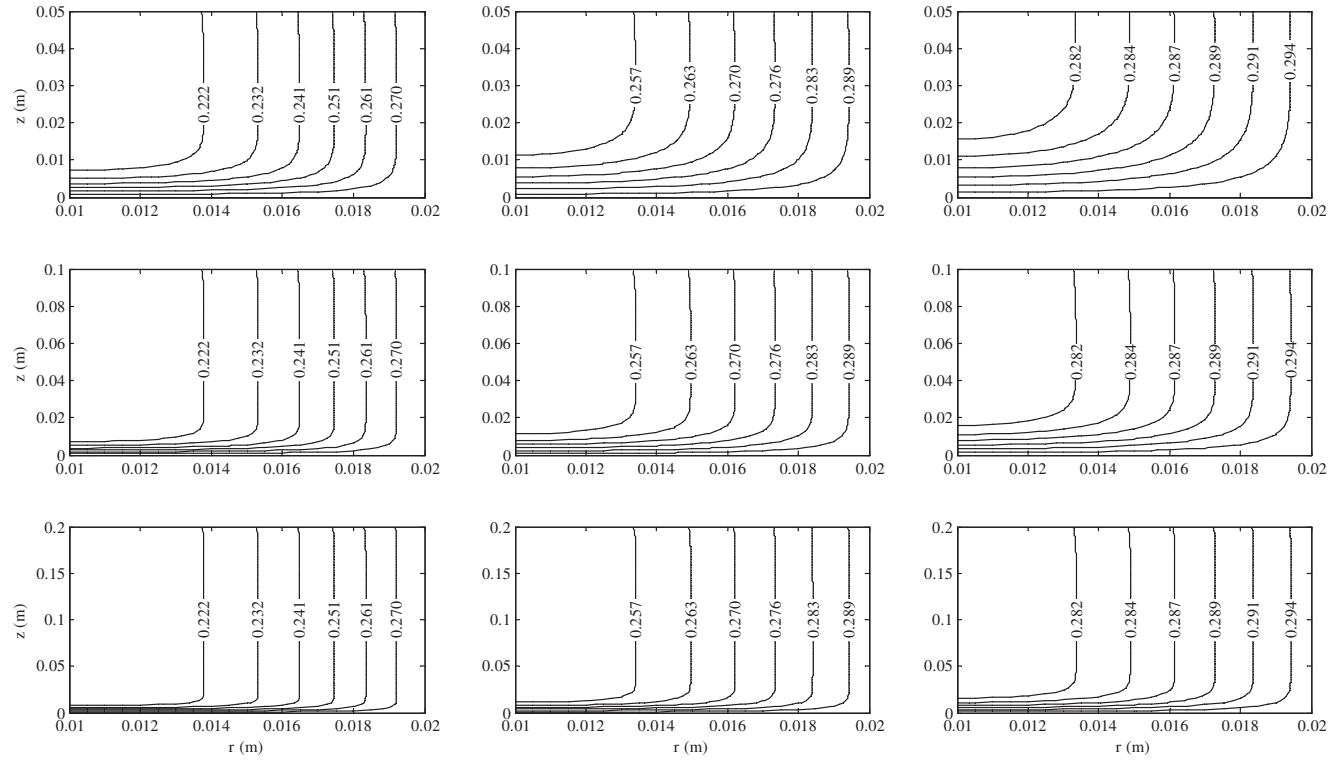

Fig. 7. Transient adsorbate concentration, $kg_w\ kg_{ad}^{-1}$, distribution for various adsorbent bed lengths. [1st row L = 0.05 m, 2nd row L = 0.1 m, 3rd row L = 0.2 m and 1st column t = 300 s, 2nd column t = 900 s, 3rd column t = 1800 s.]

move from the high pressure to low pressure regions. As a result of this, the adsorbate concentration at the outer boundaries increases suddenly. After half an hour, the adsorbent bed nearly reaches thermal, mechanical and chemical equilibrium conditions.

5.4. Adsorbent bed thickness

The influence of the adsorbent bed thickness on the distributions of the solid phase temperature, pressure and adsorbate concentration are presented in Figs. 8–10, respectively. The adsorbent bed thickness has a great influence on the temperature and adsorbate concentration distributions. The heat and mass transfer inside the adsorbent bed depend strongly on the radius when the adsorbent bed thickness is decreased for the given adsorbent bed length. However, the pressure distribution is only slightly affected by the variations in the adsorbent bed thickness, and generally the uniform pressure assumption is valid. The bed approaches thermal, mechanical and chemical equilibrium conditions after 600, 1800 and 3700 s for adsorbent bed thickness 0.005, 0.01 and 0.015 m, respectively. The reason behind this result is that the thermal resistance inside the adsorbent bed increases with increases in the adsorbent bed thickness and this results in longer times to equilibrium. Therefore, the adsorbent bed thickness should be kept as small as possible to improve the heat transfer conditions and as result, reduce the process time. However, this conclusion is based on the assumption that the mass of the shell is neglected. Additionally, it is quite obvious in Fig. 8 that the adsorbent bed thickness ($R_o - R_i$) should not be >0.01 m for good heat transfer characteristics. Improving the heat transfer conditions makes it possible to reach the chemical equilibrium condition in a shorter time as well since the adsorbate concentration is mainly a function of temperature and pressure.

5.5. Convective heat transfer coefficient

The variation of the solid phase temperature, pressure, and adsorbate concentration inside the adsorbent bed for values of the convective heat transfer coefficient between the adsorbent bed and heat transfer fluid of 25, 200 and 400 $W\,m^{-2}K^{-1}$ at times of 600, 1200, and 2000 s are presented in Figs. 11–13, respectively. The simulations were terminated after 2000 s as the system was close to equilibrium. The temperature distribution, and thus pressure and adsorbate concentration distributions as well, are nearly insensitive to the variation of the convective heat transfer coefficient due to the low thermal conductivity of the adsorbent material. The pressure distribution throughout the adsorbent bed is generally uniform except at early time steps of the process. This is due to the fact that the temperatures of the solid and gas phases near the heat transfer boundaries decreases under the given boundary conditions and as a result of this the adsorbate concentration increases and the pressure decreases. Consequently, the pressure gradients inside the adsorbent bed becomes significant and adsorbate vapor flows from high pressure to low pressure regions and thus the pressure also decreases at the adiabatic boundaries. In terms of the thermal response of the system little benefit is seen in increasing the value of the convective heat transfer coefficient above 200 $W\,m^{-2}K^{-1}$ since there is not any significant difference between the 200 and 400 $W\,m^{-2}K^{-1}$ in terms of temperature, pressure and adsorbate concentration distributions.

5.6. Thermal conductivity of the solid adsorbent material

The variation of the solid phase temperature, pressure and adsorbate concentration inside the adsorbent bed at 150, 300 and 500 s for thermal conductivities of the solid adsorbent material of 0.2, 0.75 and 1.5 $W\,m^{-1}K^{-1}$ are shown in Fig. 14–16, respectively. It is clear in Fig. 14 that heat transfer conditions inside the adsorbent bed are affected positively by increases in the solid phase thermal conductivity. Temperature gradients in the both directions decrease when the thermal conductivity of the solid adsorbent material is increased. The thermal equilibrium condition (maximum temperature difference within the bed is <3 °C) is

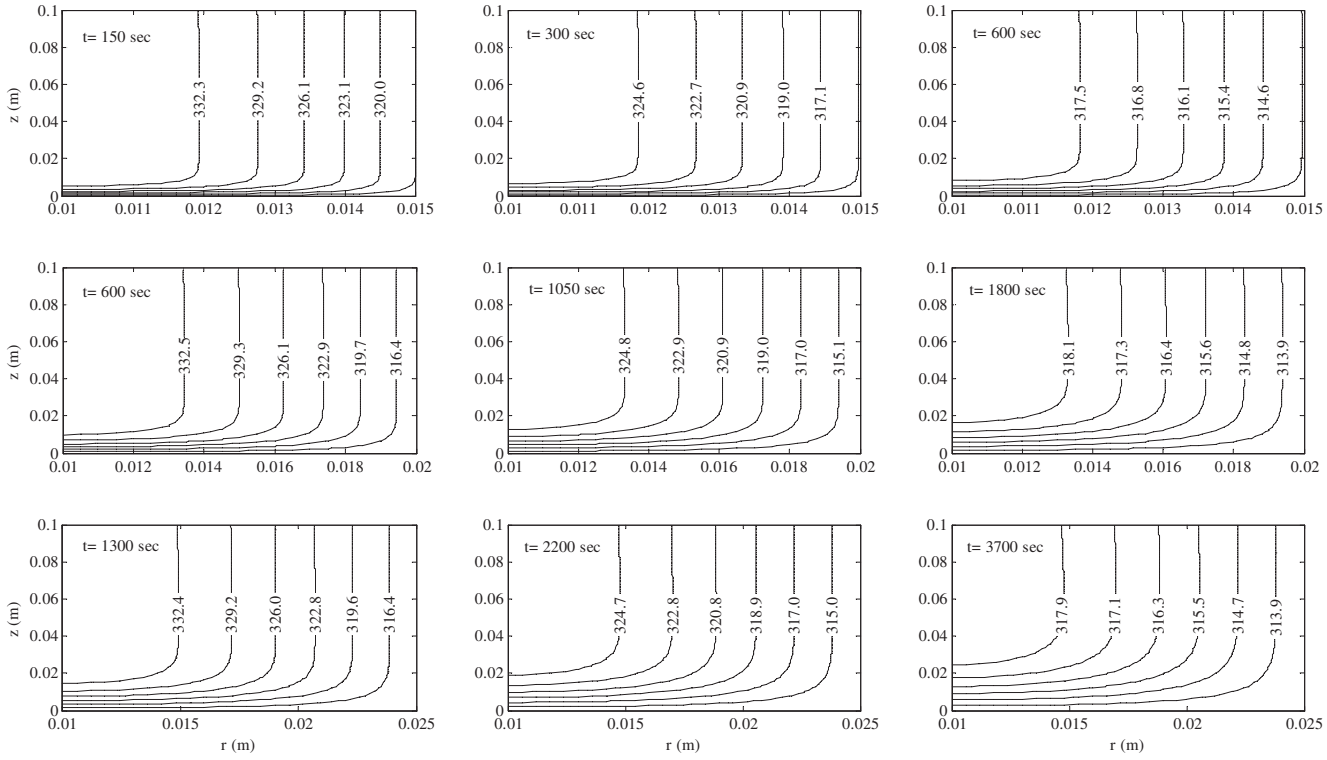

Fig. 8. Transient solid phase temperature, *K*, distribution for various adsorbent bed thicknesses. [1st row R_o = 0.015 m, 2nd row R_o = 0.02 m, 3rd row R_o = 0.025 m.]

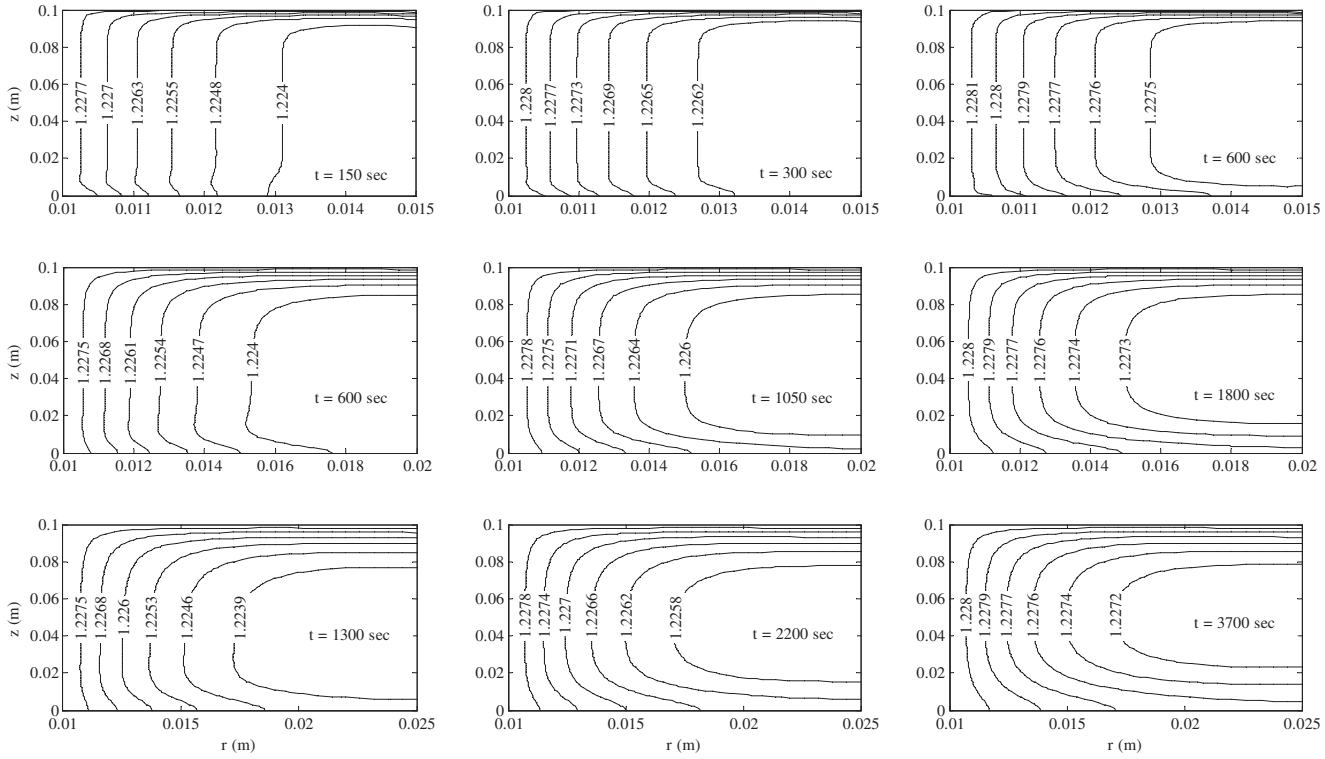

Fig. 9. Transient pressure, kPa, distribution for various adsorbent bed thicknesses. [1st row R_o = 0.015 m, 2nd row R_o = 0.02 m, 3rd row R_o = 0.025 m.]

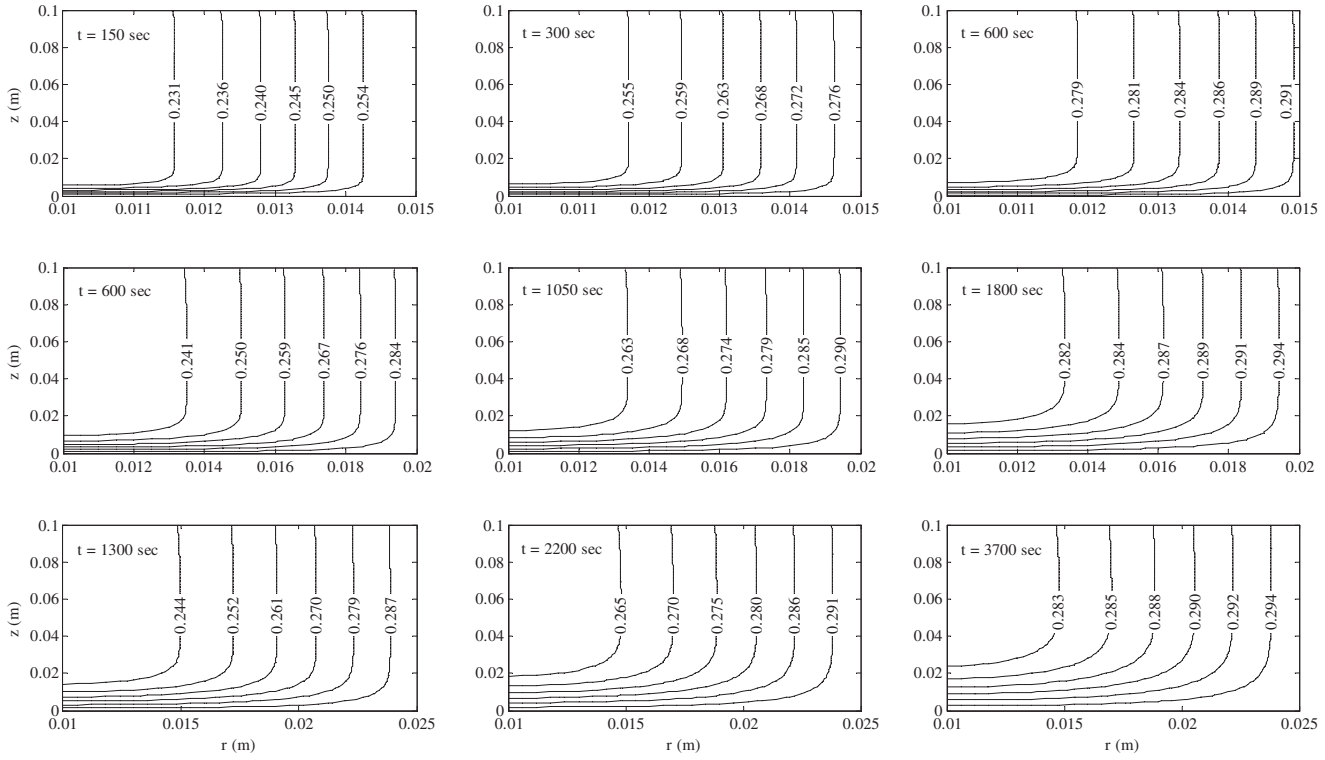

Fig. 10. Transient adsorbate concentration, $kg_w\ kg_{ad}^{-1}$, distribution for various adsorbent bed thicknesses. [1st row R_o = 0.015 m, 2nd row R_o = 0.02 m, 3rd row R_o = 0.025 m.]

nearly satisfied for the adsorbent bed having a thermal conductivity of 1.5 $W\ m^{-1}K^{-1}$ for process times equal to 500 s. However, at this time instant, temperature gradients are comparatively high for a thermal conductivity of 0.2 $W\ m^{-1}K^{-1}$. Therefore, the specific cooling power of the adsorption cooling system can be improved considerably by eliminating the limiting effects of the heat transfer

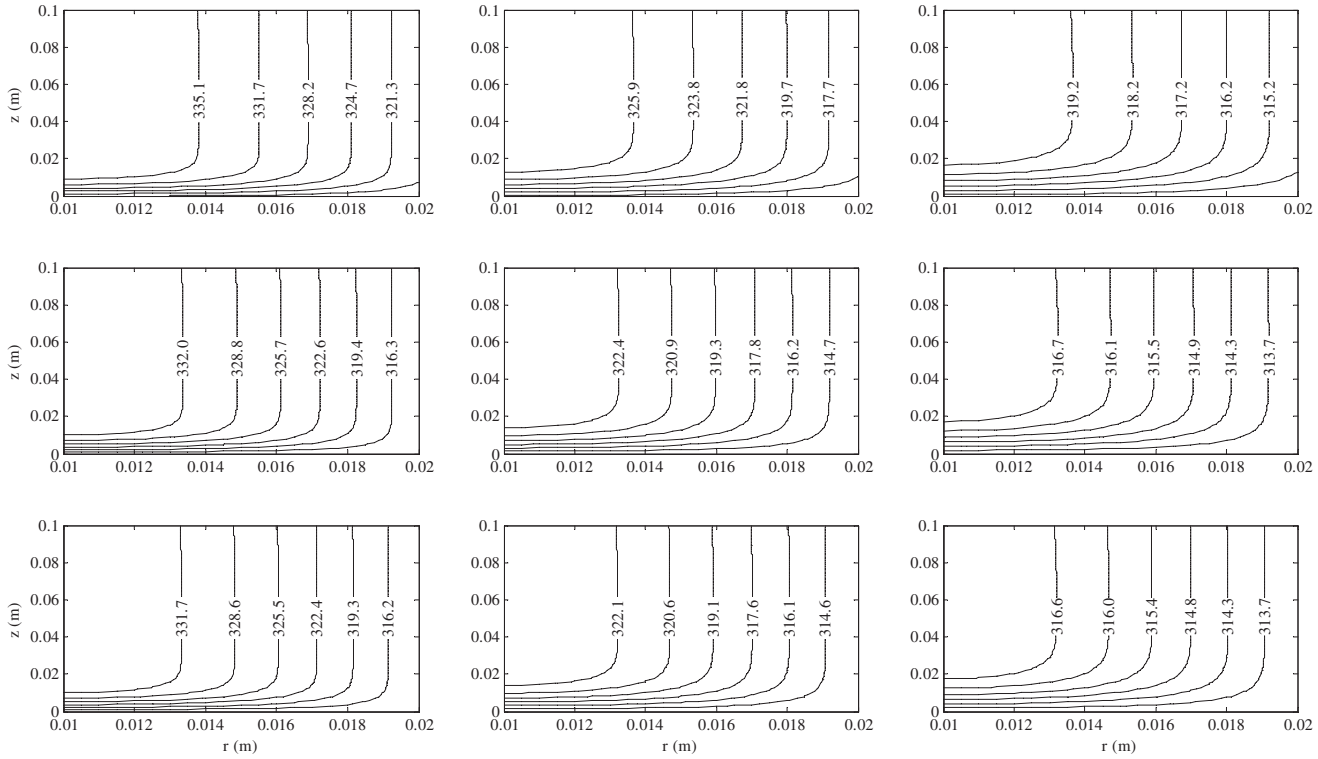

Fig. 11. Transient solid phase temperature, *K*, distribution for three convective heat transfer coefficients and times. [1st row $h = 25\ \mathrm{W\,m^{-2}K^{-1}}$, 2nd row $h = 200\ \mathrm{W\,m^{-2}K^{-1}}$, 3rd row $h = 400\ \mathrm{W\,m^{-2}K^{-1}}$and 1st column $t = 600$ s, 2nd column $t = 1200$ s, 3rd column $t = 2000$ s.]

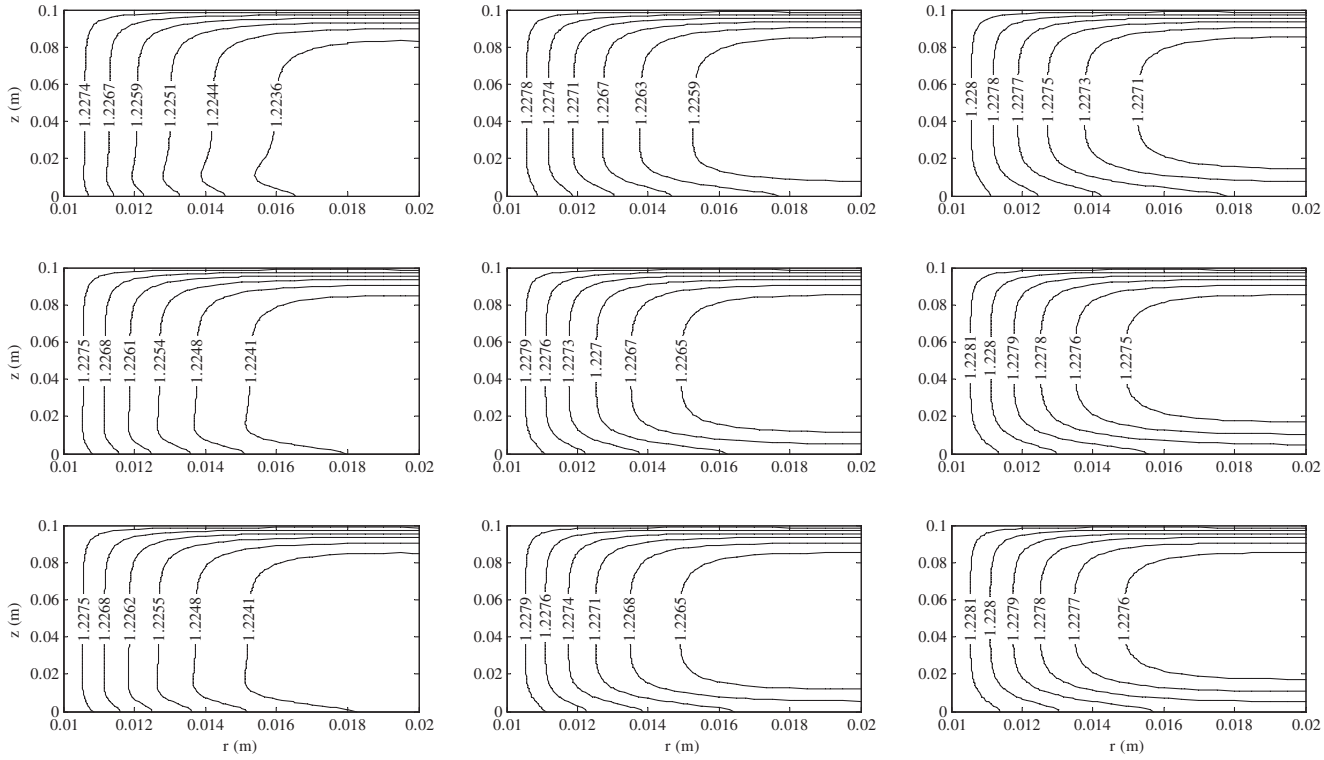

Fig. 12. Transient pressure, kPa, distribution for three convective heat transfer coefficients and times. [1st row $h = 25\ \mathrm{W\,m^{-2}K^{-1}}$, 2nd row $h = 200\ \mathrm{W\,m^{-2}K^{-1}}$, 3rd row $h = 400\ \mathrm{W\,m^{-2}K^{-1}}$and 1st column $t = 600$ s, 2nd column $t = 1200$ s, 3rd column $t = 2000$ s.]

rate inside the adsorbent bed. Pressure distributions for the three cases are generally uniform but the pressure distribution for the $k = 1.5\ W\,m^{-1}K^{-1}$ is slightly less than the others at early time steps of the process due to the high adsorption rate. This is due to the fact that the heat transfer rate is comparatively high and this results in a sudden temperature drop inside the adsorbent bed. As

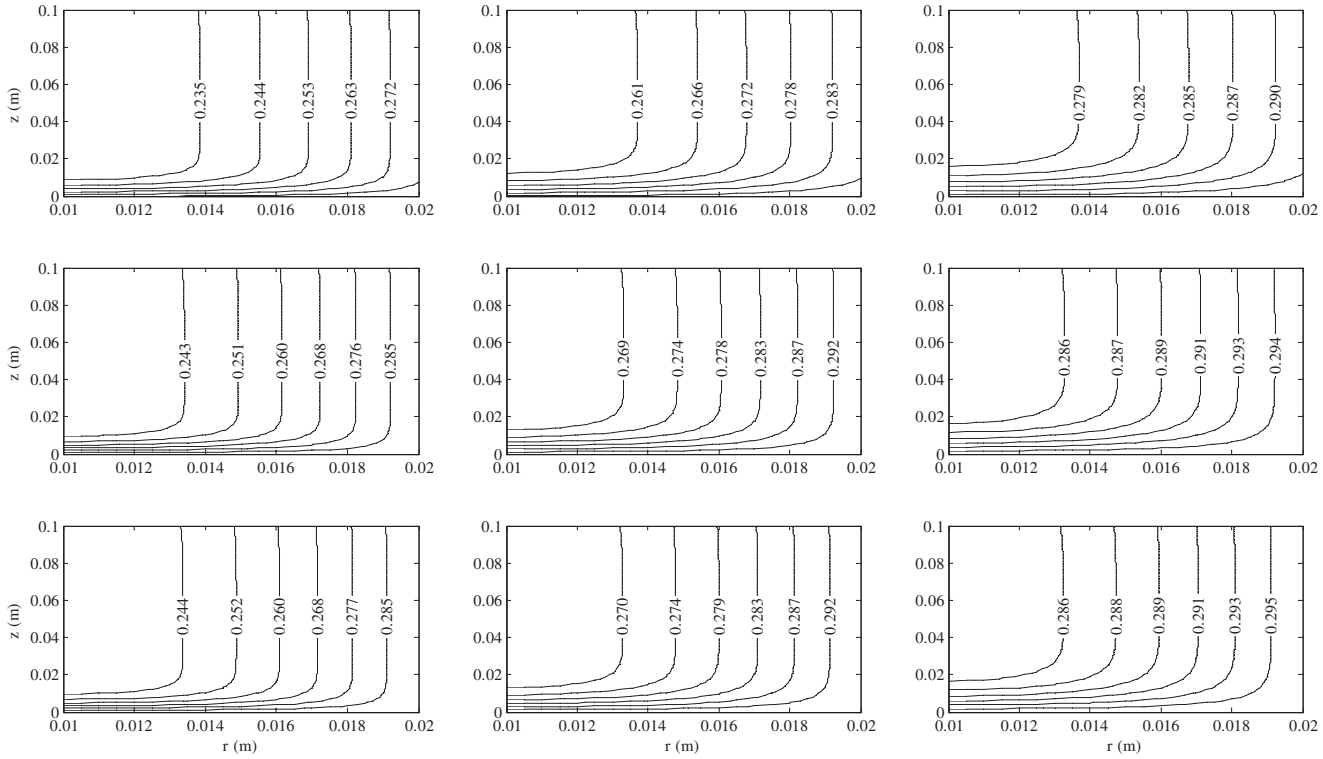

Fig. 13. Transient adsorbate concentration, $kg_w\,kg_{ad}^{-1}$, distribution for three convective heat transfer coefficients and times. [1st row $h = 25\ W\,m^{-2}K^{-1}$, 2nd row $h = 200\ W\,m^{-2}K^{-1}$, 3rd row $h = 400\ W\,m^{-2}K^{-1}$and 1st column $t = 600$ s, 2nd column $t = 1200$ s, 3rd column $t = 2000$ s.]

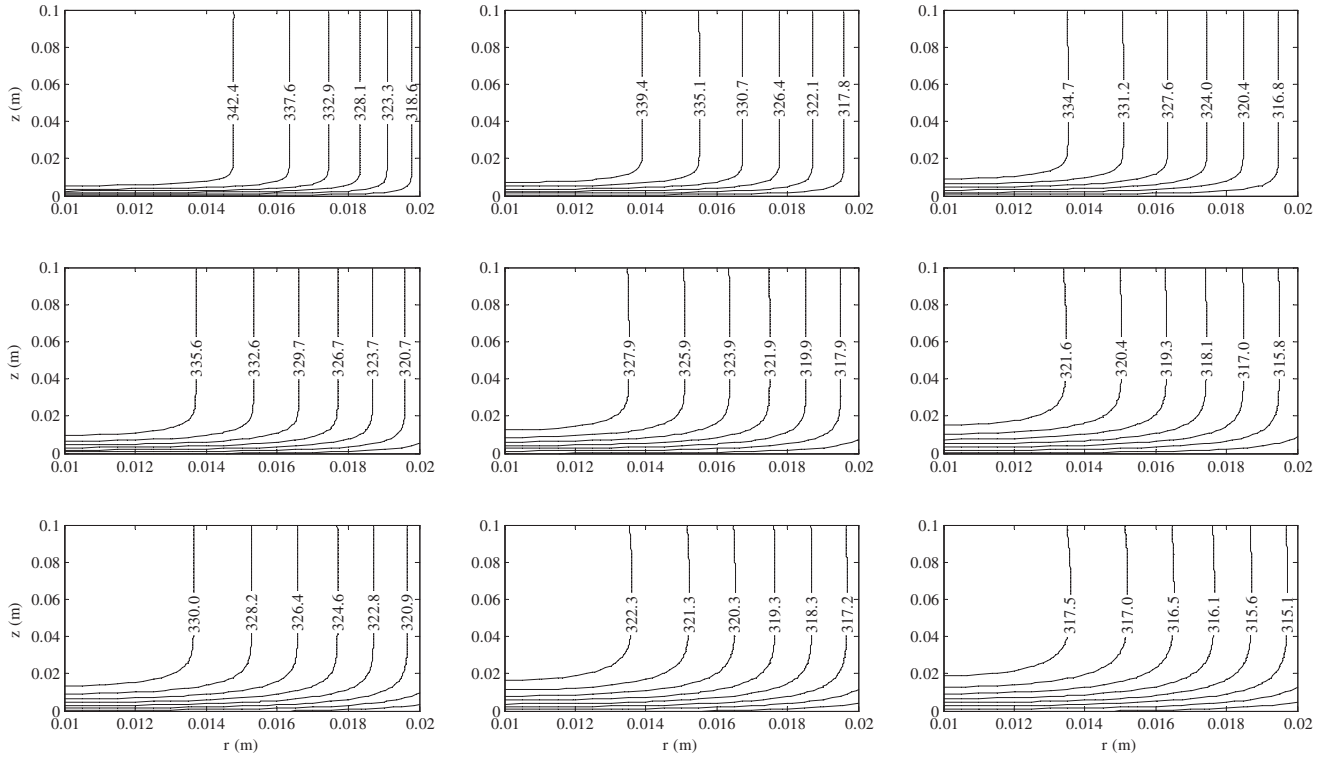

Fig. 14. Transient solid phase temperature, K, distribution for various adsorbent material conductivity. [1st row $k_s = 0.2\ W\,m^{-1}K^{-1}$, 2nd row $k_s = 0.75\ W\,m^{-1}K^{-1}$, 3rd row $k_s = 1.5\ W\,m^{-1}K^{-1}$ and 1st column $t = 150$ s, 2nd column $t = 300$ s, 3rd column $t = 500$ s.]

a result of this, the adsorption rate increases and the pressure decreases, and this pressure drop is not compensated for by an increase in the vapor diffusion flux. Adsorption equilibrium condition inside the adsorbent bed is achieved in a comparatively short period of time when the thermal conductivity of the solid adsorbent material is high.

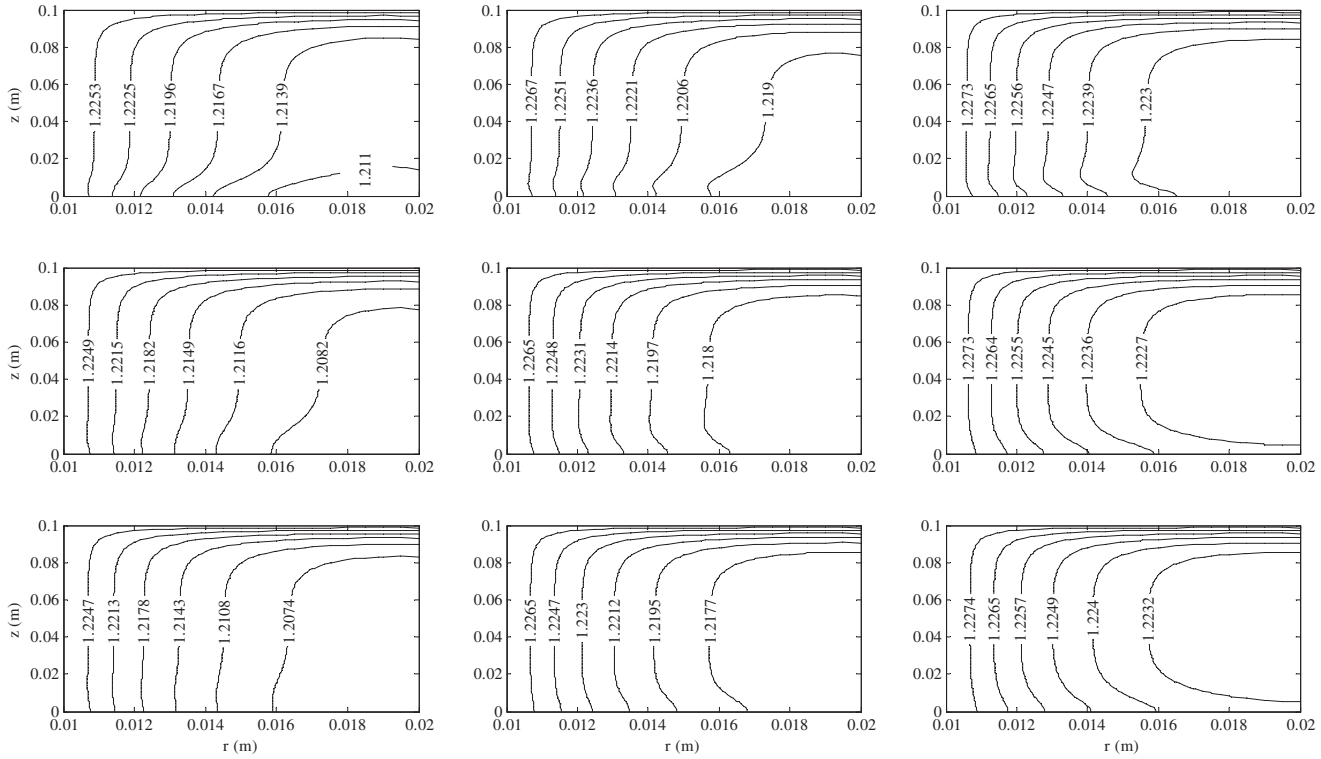

Fig. 15. Transient pressure, kPa, distribution for various adsorbent material conductivity. [1st row k_s = 0.2 W m^{-1}K^{-1}, 2nd row k_s = 0.75 W m^{-1}K^{-1}, 3rd row k_s = 1.5 W m^{-1}K^{-1} and 1st column t = 150 s, 2nd column t = 300 s, 3rd column t = 500 s.]

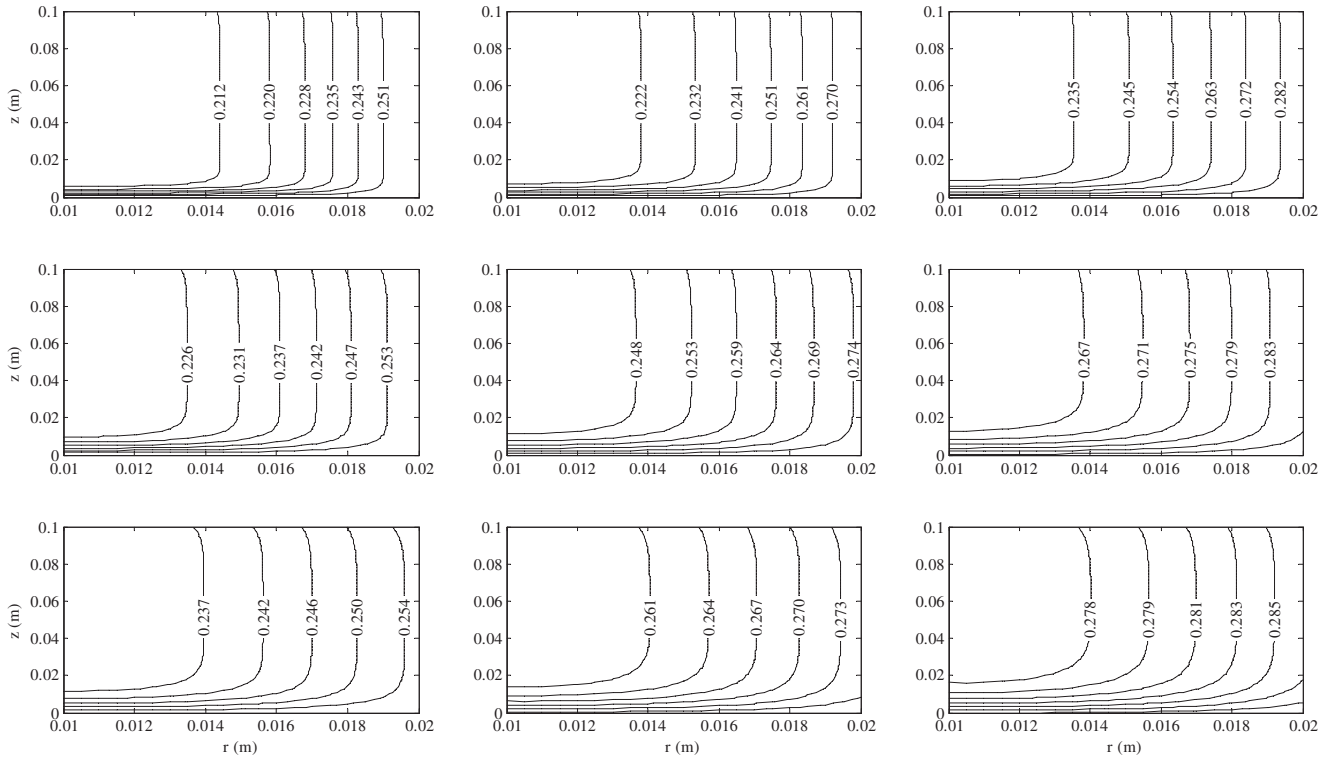

Fig. 16. Transient adsorbate concentration, $kg_w\ kg_{ad}^{-1}$, distribution for various adsorbent material conductivity. [1st row k_s = 0.2 W m^{-1}K^{-1}, 2nd row k_s = 0.75 W m^{-1}K^{-1}, 3rd row k_s = 1.5 W m^{-1}K^{-1} and 1st column t = 150 s, 2nd column t = 300 s, 3rd column t = 500 s.]

6. Conclusions

Based on the numerical model developed and for the conditions explored, the conclusions about the current study can be summarized as follows:

- The temperature difference between the solid and gas phases are generally insignificant. Hence the local thermal equilibrium assumption is generally valid. The exception is during the early stages of the process.

- The adsorbate concentration difference between the instantaneous equilibrium and LDF models is small and varies only slightly over the range of parameters investigated. Hence, the internal mass transfer resistances are negligibly small for these conditions.
- The distribution of the gas phase pressure inside adsorbent bed does not vary significantly for all the cases and thus, a spatially isobaric bed assumption can be accepted without leading to any significant computational errors.
- The heat and mass transfer inside the adsorbent bed occurs almost exclusively in the radial direction when the ratio of the adsorbent length over adsorbent bed thickness is >10.
- The adsorbent bed thickness has a large impact on the heat and mass transfer inside the adsorbent bed. The adsorbent bed thickness should not be more than 0.01 m for good heat transfer rates and hence, shorter cycle times. The heat and mass transfer gradually becomes one dimensional (almost only in the r direction) when the adsorbent bed thickness is decreased for a fixed adsorbent bed length.
- The heat and mass transfer inside adsorbent bed is nearly insensitive to variations in the heat transfer fluid convective heat transfer coefficient since the thermal conductivity of the solid adsorbent material is low. Therefore, based on heat and mass transfer considerations the value of the convective heat transfer coefficient does not need to be more than 200 $W\,m^{-2}K^{-1}$ since increasing value of the convective heat transfer coefficient (>200 $W\,m^{-2}K^{-1}$) does not lead to any significant decrease in the temperature, pressure and adsorbate concentration gradients.
- The solid phase thermal conductivity has a strong influence on the heat and mass transfer conditions inside the adsorbent bed and both conditions can be improved considerably by using highly conductive adsorbent materials, fins, or other thermal enhancements.

Acknowledgment

İsmail Solmuş would like to thank The Scientific & Technological Research Council of Turkey (TÜBİTAK) and the Middle East Technical University for supporting him with a fellowship during his study at the University of Bath in the United Kingdom.

References

[1] J.M. Calm, Emissions and environmental impacts from air-conditioning and refrigeration systems, Int. J. Refrig. 25 (2002) 293–305.
[2] M. Izquierdoa, A. Moreno-Rodrígueza, A. González-Gilb, N. García-Hernandoa, Air conditioning in the region of Madrid, Spain: an approach to electricity consumption, economics and CO_2 emissions, Energy 36 (2011) 1630–1639.
[3] A. Avgelis, A.M. Papadopoulosa, Application of multicriteria analysis in designing HVAC systems, Energy Build. 41 (2009) 774–780.
[4] D.S. Kim, C.A. Infante Ferreira, Solar refrigeration options – a state-of-the-art review, Int. J. Refrig. 31 (2008) 3–15.
[5] M. Asifa, T. Muneer, Energy supply, its demand and security issues for developed and emerging economies, Renewable Sustainable Energy Rev. 11 (2007) 1388–1413.
[6] C.A. Balaras, G. Grossman, H.M. Henning, C.A.I. Ferreira, E. Podesser, L. Wang, E. Wiemken, Solar air conditioning in Europe-an overview, Renewable Sustainable Energy Rev. 11 (2007) 299–314.
[7] A.O. Dieng, R.Z. Wang, Literature review on solar adsorption technologies for ice-making and air-conditioning purposes and recent developments in solar technology, Renewable Sustainable Energy Rev. 5 (2001) 313–342.
[8] F. Duval, F. Fichot, M. Quintard, A local thermal non-equilibrium model for two-phase flows with phase-change in porous media, Int. J. Heat Mass Transfer 47 (2004) 613–639.
[9] L.Z. Zhang, L. Wang, Effects of coupled heat and mass transfers in adsorbent on the performance of a waste heat adsorption cooling unit, Appl. Therm. Eng. 19 (1999) 195–215.
[10] L.Z. Zhang, A three dimensional non-equilibrium model for an intermittent adsorption cooling system, Sol. Energy 69 (2000) 27–35.
[11] Y.J. Dai, K. Sumathy, Heat and mass transfer in the adsorbent of a solar adsorption cooling system with glass tube insulation, Energy 28 (2003) 1511–1527.
[12] M.H. Chahbani, J. Labidi, J. Paris, Effect of mass transfer kinetics on the performance of adsorptive heat pump systems, Appl. Therm. Eng. 22 (2002) 23–40.
[13] M.H. Chahbani, J. Labidi, J. Paris, Modeling of adsorption heat pumps with heat regeneration, Appl. Therm. Eng. 24 (2004) 431–447.
[14] A. El Fadar, A. Mimet, M. Perez-Garcia, Modeling and performance study of a continuous adsorption refrigeration system driven by parabolic trough solar collector, Sol. Energy 83 (2009) 850–861.
[15] K.C. Leong, Y. Liu, Numerical modeling of combined heat and mass transfer in the adsorbent bed of a zeolite/water cooling system, Appl. Therm. Eng. 24 (2004) 2359–2374.
[16] K.C. Leong, Y. Liu, Numerical study of a combined heat and mass recovery adsorption cooling cycle, Int. J. Heat Mass Transfer 47 (2004) 4761–4770.
[17] K.C. Leong, Y. Liu, System performance of a combined heat and mass recovery adsorption cooling cycle: a parametric study, Int. J. Heat Mass Transfer 49 (2006) 2703–2711.
[18] Y. Liu, K.C. Leong, The effect of operating conditions on the performance of zeolite/water adsorption cooling systems, Appl. Therm. Eng. 25 (2005) 1403–1418.
[19] W.D. Wu, H. Zhang, D.W. Sun, Mathematical simulation and experimental study of a modified zeolite 13X–water adsorption refrigeration module, Appl. Therm. Eng. 29 (2009) 645–651.
[20] G. Maggio, A. Freni, G. Restuccia, A dynamic model of heat and mass transfer in a double-bed adsorption machine with internal heat recovery, Int. J. Refrig. 29 (2006) 589–600.
[21] L. Marletta, G. Maggio, A. Freni, M. Ingrasciotta, G. Restuccia, A non-uniform temperature non-uniform pressure dynamic model of heat and mass transfer in compact adsorbent beds, Int. J. Heat Mass Transfer 45 (2002) 3321–3330.
[22] L.M. Sun, Y. Feng, M. Pons, Numerical investigation of adsorptive heat pump systems with thermal wave heat regeneration under uniform-pressure conditions, Int. J. Heat Mass Transfer 40 (1997) 281–293.
[23] M. Li, R.Z. Wang, Heat and mass transfer in a flat plate solar solid adsorption refrigeration ice maker, Renewable Energy 28 (2003) 613–622.
[24] Y. Pei-Zhi, Heat and mass transfer in adsorbent bed with consideration of non-equilibrium adsorption, Appl. Therm. Eng. 29 (2009) 3198–3203.
[25] A. Mhimid, Theoretical study of heat and mass transfer in a zeolite bed during water desorption: validity of local thermal equilibrium assumption, Int. J. Heat Mass Transfer 41 (1998) 2967–2977.
[26] A. Jemni, S.B. Nasrallah, Study of two-dimensional heat and mass transfer during absorption in a metal-hydrogen reactor, Int. J. Hydrogen Energy 20 (1995) 43–52.
[27] J.J. Guilleminot, F. Meunier, Heat and mass transfer in a non-isothermal fixed bed solid adsorbent reactor: a uniform pressure non-uniform temperature case, Int. J. Heat Mass Transfer 30 (1987) 1595–1606.
[28] L. Yong, K. Sumathy, Comparison between heat transfer and heat mass transfer models for transportation process in an adsorbent bed, Int. J. Heat Mass Transfer 47 (2004) 1587–1598.
[29] H. Demir, M. Mobedi, S. Ülkü, Effect of porosity on heat and mass transfer in a granular adsorbent bed, Int. Commun. Heat Mass Transfer 36 (2009) 372–377.
[30] J. Hager, R. Wimmerstedt, S. Whitaker, Steam drying a bed of porous spheres: theory and experiment, Chem. Eng. Sci. 55 (2000) 1675–1698.
[31] D.A. Nield, A. Bejan, Convection in Porous Media, second ed., Springer, 1999.
[32] M. Sözen, K. Vafai, Analysis of the non-thermal equilibrium condensing flow of a gas through a packed bed, Int. J. Heat Mass Transfer 33 (1990) 1247–1261.
[33] J. Di, J.Y. Wu, Z.Z. Xia, R.Z. Wang, Theoretical and experimental study on characteristics of a novel silica gel-water chiller under the conditions of variable heat source temperature, Int. J. Refrig. 30 (2007) 515–526.
[34] H.T. Chua, K.C. Ng, W. Wang, C. Yap, X.L. Wang, Transient modeling of a two-bed silica gel–water adsorption chiller, Int. J. Heat Mass Transfer 47 (2004) 659–669.